In Situ TEM Study of Lithiation Behavior of Silicon Nanoparticles Attached to and Embedded in a Carbon Matrix

Meng Gu,[†] Ying Li,[‡] Xiaolin Li,[§] Shenyang Hu,[⊥] Xiangwu Zhang,[‡] Wu Xu,[⊥] Suntharampillai Thevuthasan,[†] Donald R. Baer,[†] Ji-Guang Zhang,[⊥] Jun Liu,[§] and Chongmin Wang[†,*]

[†]Environmental Molecular Sciences Laboratory, Pacific Northwest National Laboratory, Richland, Washington 99352, United States , [‡]Fiber and Polymer Science Program, Department of Textile Engineering, Chemistry and Science, North Carolina State University, Raleigh, North Carolina 27695-8301, United States , [§]Fundamental and Computational Science Directorate, Pacific Northwest National Laboratory, Richland, Washington 99352, United States , and [⊥]Energy and Environmental Directorate, Pacific Northwest National Laboratory, Richland, Washington 99352, United States

ABSTRACT Rational design of silicon and carbon nanocomposite with a special topological feature has been demonstrated to be a feasible way for mitigating the capacity fading associated with the large volume change of silicon anode in lithium ion batteries. Although the lithiation behavior of silicon and carbon as individual components has been well understood, lithium ion transport behavior across a network of silicon and carbon is still lacking. In this paper, we probe the lithiation behavior of silicon nanoparticles attached to and embedded in a carbon nanofiber using *in situ* TEM and continuum mechanical calculation. We found that aggregated silicon nanoparticles show contact flattening upon initial lithiation, which is characteristically analogous to the classic sintering of powder particles by a neck-growth mechanism. As compared with the surface-attached silicon particles, particles embedded in the carbon matrix show delayed lithiation. Depending on the strength of the carbon matrix, lithiation of the embedded silicon nanoparticles can lead to the fracture of the carbon fiber. These observations provide insights on lithium ion transport in the network-structured composite of silicon and carbon and ultimately provide fundamental guidance for mitigating the failure of batteries due to the large volume change of silicon anodes.

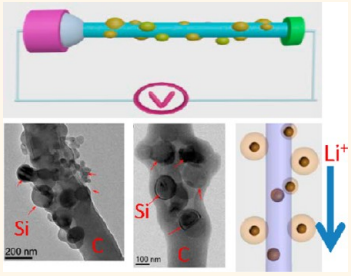

KEYWORDS: Si nanoparticle · carbon fiber · Li-ion battery · *in situ* TEM · lithiation · fracture

Li-ion batteries with excellent energy conversion efficiency and high energy density have been widely used in portable electronics and mobile communication devices and have started to enter the plug-in hybrid vehicle and electrical vehicle markets. In addition, the successful exploration of sustainable energy sources, such as solar and wind energy, depends greatly on the utilization of Li-ion batteries as efficient energy storage devices. Silicon is a promising candidate as an anode material for next-generation Li-ion batteries due to its superior capacity, with a gravimetric capacity of ~4200 mAh g^{-1} and a volumetric capacity of ~8500 mAh cm^{-3}.[1−9] Upon lithiation, Si will expand by 300% with dramatic anisotropic change, showing obvious elongation along the [110] direction for crystalline Si.[10−14] Associated with such a large anisotropic volume expansion, the silicon anode materials are subject to pulverization, leading to the loss of electrical contact and rapid capacity fading of the battery.

With the general guidance of continuum mechanics on the deformation and fracture behavior of silicon upon lithiation, numerous fundamental microstructure design concepts have emerged for mitigating the failure of the silicon anode caused by large volume changes.[15,16] Two strategies have been used: (1) The first is tailoring of Si to a low dimension with special topological features. Typical examples for this strategy include silicon nanowires,[4,10,12,17] nanorods,[8] nanotubes,[3] crystalline or amorphous silicon films,[2,18] hollow-structure silicon balls,[19] and double-wall silicon nanotubes.[20] Lithium ion batteries with a double-wall silicon nanotube anode have been demonstrated to be able to charge/discharge up to several thousand times with high capacity retention.[20] (2) The second strategy is making silicon-based composite materials. Carbon is a commonly used conductive additive in lithium electrode materials and has a variety of structures, ranging from particles to tubes, fibers, and even a single layer as graphene.[21−23]

* Address correspondence to Chongmin.Wang@pnnl.gov.

Received for review July 23, 2012 and accepted August 23, 2012.

Published online August 23, 2012
10.1021/nn303312m

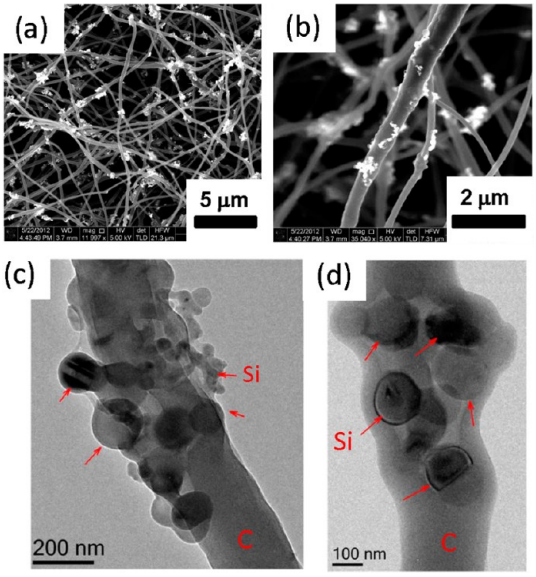

Figure 1. SEM and TEM images showing the general microstructure of the silicon nanoparticles and CNF composite. (a) SEM image of overall view in which the silicon nanoparticles appear as white clusters. (b) SEM showing the cluster of silicon nanoparticles on a CNF. (c) TEM image showing the surface-attached silicon nanoparticles. (d) TEM image showing a cluster of silicon nanoparticles embedded in the CNF.

Therefore, it is a natural approach to rationally design a composite material based on silicon and carbon.[24−36] One of the key concerns for this type of composite material is the lithium ion transport behavior across the network structure of silicon and carbon as well as the accommodation of the volume change of the silicon upon lithiation. Here, we performed an in-depth study on the lithiation behavior of Si nanoparticles and a carbon nanofiber composite, which are composed of crystalline Si nanoparticles attached to and embedded in a carbon fiber using *in situ* transmission electron microscopy (TEM).[34,37] The information acquired allows us to elucidate the failure mechanism and limiting factors in designing anode materials based on silicon and carbon composites.[27,34,37,38]

RESULTS AND DISCUSSION

The overall structural features of the Si-CNF are revealed by the scanning electron microscopy (SEM) and TEM images shown in Figure 1. The diameter of the carbon nanofiber (CNF) ranges from 150 to 300 nm. The size of the silicon nanoparticles varies from 60 to 100 nm in diameter. Microscopically, the majority of the silicon nanoparticles aggregate to form particle clusters, which are either attached to the surface of the CNF (Figure 1c) or embedded in the CNF (Figure 1d). We also noticed that in some regions there are isolated silicon nanoparticles either attached to or embedded in the CNF.

The lithiation-induced microstructural evolution of the silicon nanoparticles attached to a CNF is illustrated by the captured video frames shown in Figure 2 as well as Movie 1 in the Supporting Information. Within the view, two clusters of particles can be seen. One cluster consists of three particles, labeled p1, p2, and p3, and the other cluster includes two particles, labeled p4 and p5. Upon lithiation, the microstructure evolution of the particles can be summarized with the following five features. (1) The ionic liquid electrolyte wetted the surface of the particles as shown in the 0 min image in Figure 2. (2) The lithiation initiates from the surface of the particle and proceeds toward the center of the particle, featuring the propagation of a boundary between the amorphous Li_xSi and crystalline Si as previously reported.[39] (3) With the progression of lithiation, the lithiation speed decreases. To illustrate this, the lithiated shell thickness as a function time is drawn in Figure 2b for p1, p3, and p4, which shows a characteristic parabolic behavior, which appears to be consistent with the general argument that the lithiation is a lithium diffusion controlled reaction. However, a detailed experimental and theoretical analysis has indicated that the lithiation of Si is an interface reaction controlled process, which should give a constant lithiation rate.[40] Theoretical analysis indicated that the stress field associated with the volume expansion has a dramatic effect on the lithiation behavior of the silicon nanoparticles. Essentially, if we draw the length of the reaction silicon normalized with the initial particle radius as illustrated in Figure 2c, we notice that particles of different sizes show similar rate behavior. The observed parabolic behavior is associated with the stress field within the Si core and the Li_xSi layer.[40−42] (4) One very unique feature for the silicon particles in contact is the lithiation-induced contact flattening of the particles, as illustrated in Figure 2a for the case of particles p1 and p2. As schematically drawn in Figure 3, the lithiation-induced particle contact flattening is very similar to the case of sintering of two particles through neck growth at high temperature.[43−47] Lithiation-induced contact flattening is the result of the deformation of particles through viscous flow. This will happen only for particles that are confined by the carbon fibers or other silicon particles.[13,14] Particles that are in contact but are not confined by the surroundings do not show contact flattening, as demonstrated in Movie 2 in the Supporting Information, where one particle is attached to another and both particles are lithiated but do not coalesce during lithiation. Our present observation of contact flattening appears to be consistent with the phenomenon of lithiation-induced welding of two crossing silicon nanowires reported by Karki *et al.*[48] (5) Eventually, the amorphous Li_xSi will transform to crystalline $Li_{15}Si_4$ as indicated by the appearance of

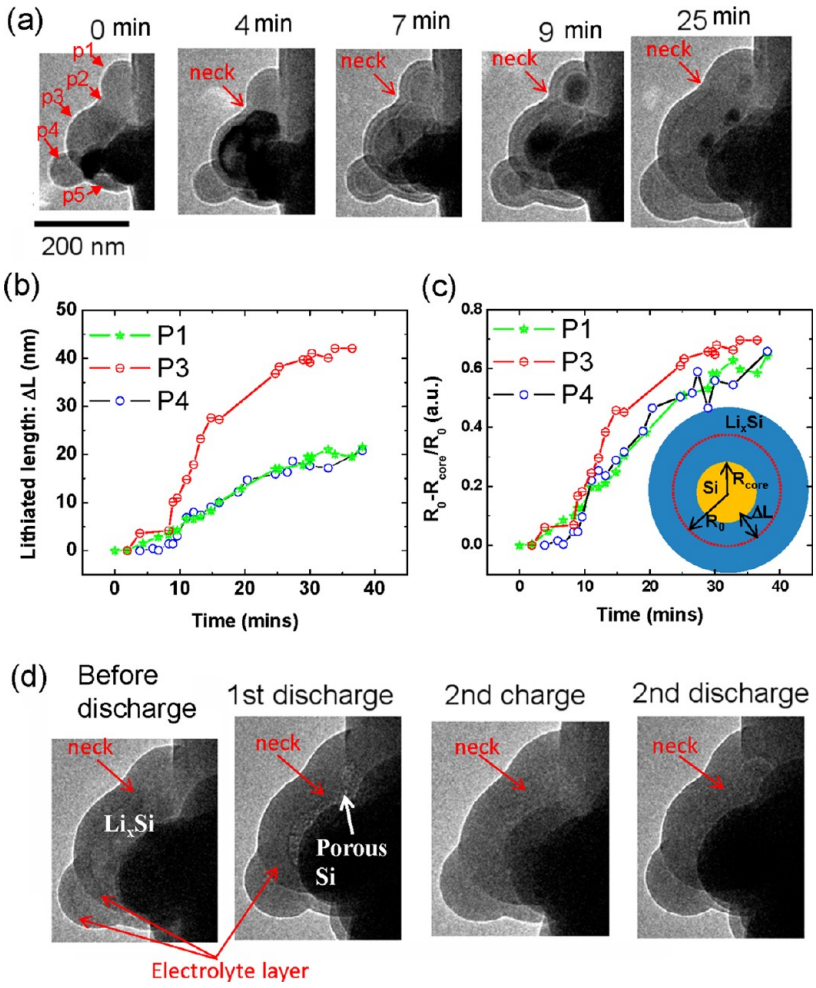

Figure 2. (a) TEM image showing microstructural evolution of the surface-attached nanoparticles. With the progression of the lithiation, p1 and p2 show contact flattening. (b) Measured lithation length, ΔL (as illustrated in the inset of (c)), as a function of time for particles p1, p3, and p4, revealing a parabolic behavior. (c) Lithiated Si as measured by ($R_0 - R_{core}$) (R_0 is the initial radius of the Si particles, R_{core} is the radius of the unlithiated Si core) is normalized with R_0 and is drawn as a function of lithation time, revealing the normalized lithiation rate is independent of the initial particle size of Si, therefore suggesting the lithiation of Si is an interface reaction controlled process. (d) Microstrucural evolution of the particles during the discharge–charge cycles shown in (a). Note the porous nature of the discharged particles.

the diffraction contrast. This phase transformation is characterized by a congruent process as discussed in detail in a prior publication.[34]

Structural evolution of the particles attached to the surface of the carbon fiber during the discharging and recharging is shown in Figure 2d. After discharging, the particles become very porous. Similar microstructural features have been observed for Si and Ge nanorods.[12,49–52] Formation of the pores is the consequence of clustering of vacancies left behind by the lithium ions during the delithiation. This likely indicates a high mobility of vacancy in the amorphous-structured Li_xSi. This is further demonstrated by a similar observation on another cluster of particles illustrated in Figure 4 and Movie 3 in the Supporting Information, where the discharged particle possesses a high porosity. Formation of the porous structure will definitely contribute to the poor capacity retention during the cyclic charge/discharge. We also noticed that the surface of the silicon particle is covered by an electrolyte layer, and the thickness of this layer increases during the charge and discharge cycles. It is not clear whether this electrolyte layer behaves like an artificial solid–electrolyte interface (SEI) layer to prevent penetration of the lithium ion during the lithiation/delithiation.

Compared with the surface-attached silicon particles, the particles embedded in the CNF show two unique features: (1) Lithiation of particles embedded in the CNF is delayed as compared to the surface-attached particles, because the lithium has to diffuse through the carbon to reach the embedded particles; (2) associated with the ~300% volume expansion upon lithiation of silicon,[11,13,14] lithiation of the particle embedded in the CNF may lead to fracture of the carbon nanofibers. These two features are vividly demonstrated by the captured video frames shown

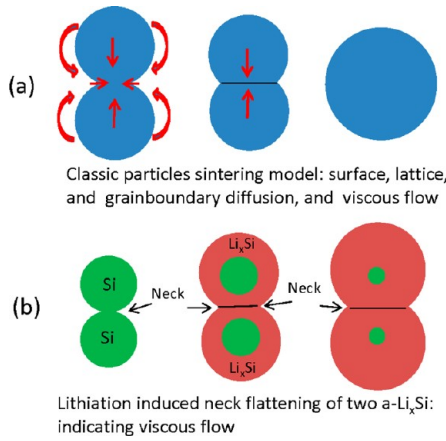

Figure 3. Analogous comparison of the classic particle sintering model with the observed contact flattening of the a-Li_xSi upon initial lithation. (a) Sintering of the two particles by surface, lattice, grain boundary diffusions, and viscous flow. The arrows in (a) indicate the mass flow by diffusion. (b) Lithiation-induced contact flattening of Li_xSi particles, which is equivalent to the coarsening of the particles.

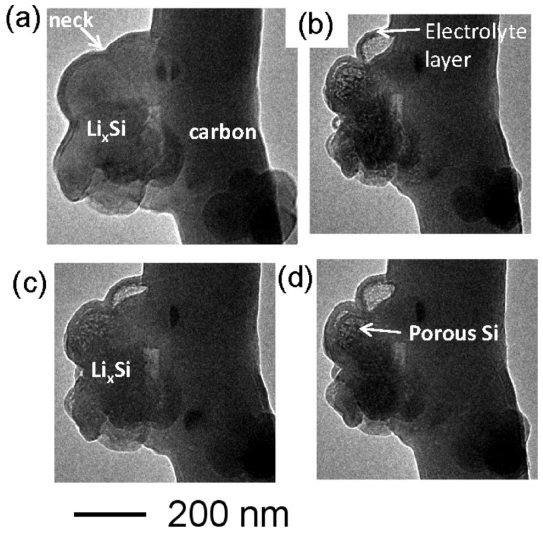

Figure 4. Formation of cavities during the discharge process: (a) 1st charged; (b) 1st discharged; (c) 2nd charged; (d) 2nd discharged.

in Figure 5 and Movie 4 in the Supporting Information. In Figure 5, several particles were attached to the outside surface of the CNF. At the same time, several particles were embedded in the carbon fiber. Upon starting of the lithiation, the particles attached to the surface of the CNF were lithiated in a core–shell fashion as described above. After ~15 min, the silicon nanoparticle embedded in the CNF begins to be lithiated. It is known that insertion of lithium into carbon-based materials causes small volume changes.[53] Therefore, it is difficult to directly monitor the diffusivity of lithium in the amorphous carbon. On the basis of the time delay of lithiation of the particles outside and inside the fiber and the diameter of the carbon fiber, it has been estimated that the lithium ion transport speed in the amorphous carbon is ~0.2 nm/s, which is contrasted with the estimated lithiation speed of 0.02 nm/s for silicon in the present case. It is known that for silicon the lithiation rate is greatly controlled by the electronic conductivity of the silicon.[54] It is reported that the lithium ion diffusivity in various composite graphite is in the range 10^{-6} to 10^{-16} cm^2/s.[55,56] Theoretical calculation indicates that for the graphitic carbon the lithium ion diffusivity along the graphene plane is ~10^{-6} to 10^{-7} cm^2/s, while along the grain boundary of the graphite composite it is about ~10^{-11} cm^2/s.[57] Apparently, the disordered structure leads to a much slower lithium transport rate as compared with that within the graphene layer.

As illustrated in Figure 5, several silicon nanoparticles were embedded in the CNF, as indicated by the arrows. Lithiation of the embedded nanoparticles leads to cracking of the carbon materials, as shown in Figure 5 and Movie 4 in the Supporting Information. Apparently, the carbon fiber shown in Figure 5 was cracked at two places, each associated with the lithiation of a single silicon nanoparticle, as indicated by the arrows. The fracture of the carbon fiber is featured by tearing along the longitudal direction of the fiber. The overall lithiation characteristics of the silicon nanoparticles attached to and embedded in CNF were schematically drawn in Figure 6. It has been observed that for a free-standing silicon particle, there exists a critical size of ~150 nm, below which the Si particle will not fracture upon lithiation.[58] For the present case, all the particles we have studied are smaller than this critical size. Therefore, we do not notice any fracture of the silicon particles either embedded or attached on the carbon fiber.

In order to quantitatively understand the fracture behavior of the carbon fiber, we calculated the stress field for the cases of silicon particles embedded in the carbon matrix (details of the calculation are described in the Supporting Information). The calculation is based on a silicon core and carbon shell spherical model as illustrated in Figure 7a. With the assumptions of elastic deformation, isotropic elastic constants, and uniform volume expansion in the lithiated layer in Si, an analytical solution of the stress field in the core–shell structure was derived as a function of the lithiated layer thickness, H. Using a theoretical volume increase of ~300% for Si upon lithiation, $R_0 = 60$ nm, $R = 120$ nm, elastic constants of Si, Young's modulus $E = 178.8$ GPa and Poisson's ratio $\nu = 0.223$, and elastic constants of carbon, $E = 820.7$ GPa and $\nu = 0.123$, the calculated radial stress (σ_{rr}) and the hoop stress ($\sigma_{\theta\theta}$ and $\sigma_{\phi\phi}$) were as illustrated in Figure 7b and c. Within the silicon particle, both σ_{rr} and $\sigma_{\theta\theta}/\sigma_{\phi\phi}$ are compressive, which in principle will not lead to the cracking of the silicon

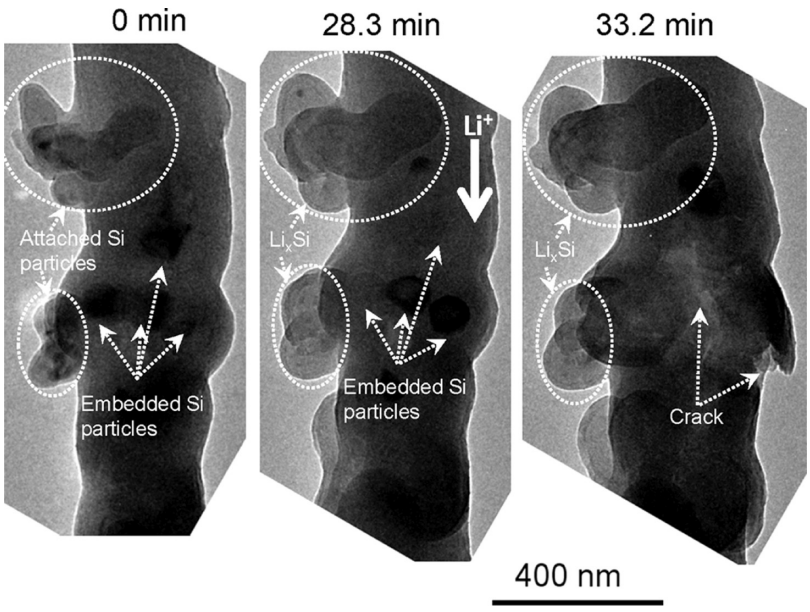

Figure 5. Comparison of the lithiation characteristics of the particles attached to and embedded in the CNF. The lilthiation of the embedded particles is delayed as compared with the particles attached to the carbon surface. Lithiation of the embedded particles leads to the cracking of the carbon fibers.

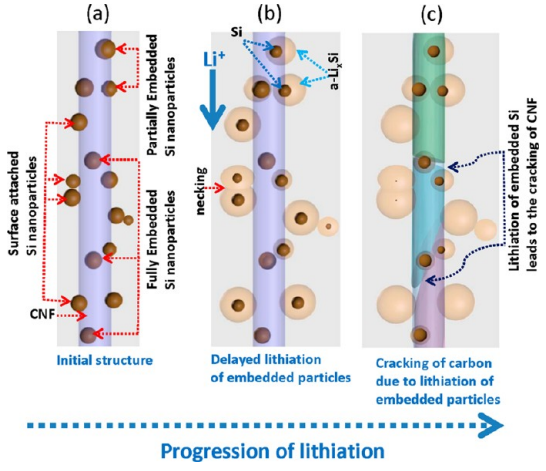

Figure 6. Schematic drawing showing the lithiation characteristics of the particles attached to and embedded in the CNF. (a) Initial structure. (b) Lithiation of the particles embedded in the CNF is delayed as compared with the particle attached to the surface of the CNF. Note the necking of the particles confined by the CNF. (c) Lithiation of the particles embedded in the CNF leads to the cracking of the CNF.

nanoparticle upon lithiation. The σ_{rr} in the carbon shell is compressive, which will not lead to the fracture of the carbon shell. The hoop stress $\sigma_{\theta\theta}$ in the carbon shell is always tensile, and it has a maximum value at the interface between the silicon core and the carbon shell. Considering the lithation of the silicon proceeds in a core−shell manner, the $\sigma_{\theta\theta}/\sigma_{\phi\phi}$ in the carbon will depend on the thickness of the lithiated layer. Figure 7b and c illustrates $\sigma_{\theta\theta}/\sigma_{\phi\phi}$ and σ_{rr} in the carbon shell for several discrete lithiated layer thicknesses. Apparently, with the increase of the lithiated layer, both σ_{rr} and $\sigma_{\theta\theta}/\sigma_{\phi\phi}$ increase. Given the factor of the tensile nature and the maximum magnitude of $\sigma_{\theta\theta}$ at the interface between the Li_xSi and the carbon shell, it would be expected that the fracture of the carbon shell will initiate from the interface. The criteria for the initiation of the fracture of the carbon shell can be generally written as $\sigma_{\theta\theta}/\sigma_{\phi\phi} \geq \sigma_c$, where σ_c is the strength of carbon materials. For typically taken $\sigma_c \approx$ 130 GPa for graphene and $\sigma_c \approx 3$ GPa for amorphous arbon fiber, Figure 7b clearly demonstrates that for amorphous carbon a lithiation layer of <10 nm will lead to the cracking of the carbon materials for the given core−shell particle. In contrast, graphene can tolerate a lithiation layer thickness of ~20 nm. It should be realized that during the lithiation of the embedded Si nanoparticles the CNF is also lithiated. It is known that lithiation of graphite lead to a 5.9% volume expansion, which is much less compared with the volume change of ~300% for the case of lithiation of Si. Therefore, for the present analysis of the stress field, plastic deformation and volume expansion of carbon are not considered. Furthermore, lithation of carbon will also lead to the modification of the mechanical property of the carbon,[53] which will correspondingly change the critical strength, σ_c, for the fracture of the carbon.

It has long been postulated that the lithiation of Si may lead to the fracture of the carbon matrix. Here we provide direct observation for such a fracture. The fracture of the carbon fiber due to the expansion of the embedded silicon nanoparticles will cause the disruption of the electron conductivity of the nanocomposite, therefore leading to the failure of

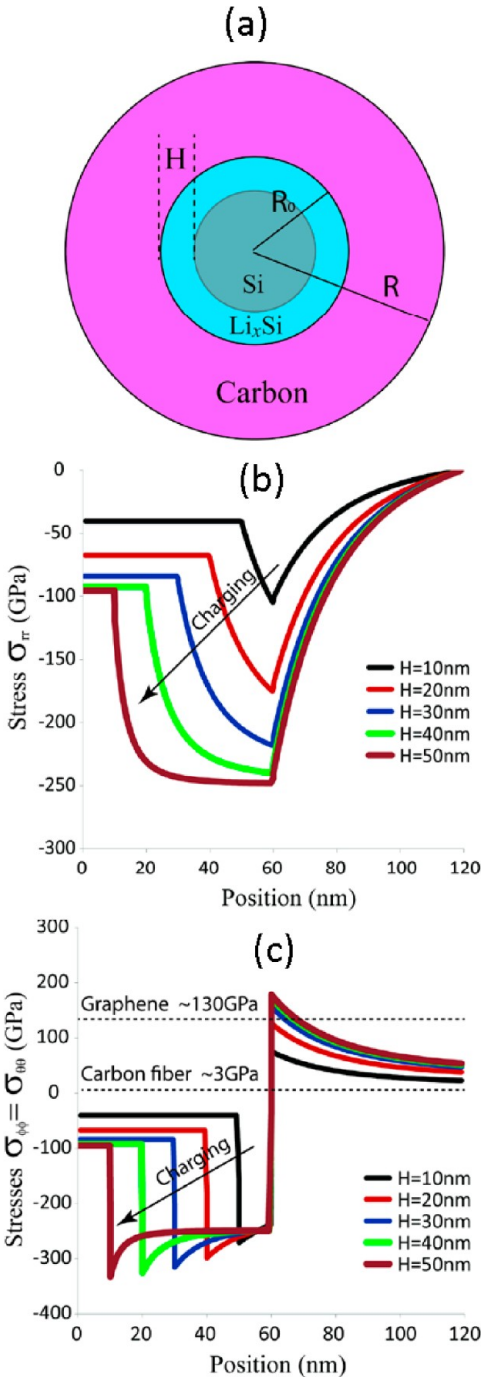

Figure 7. Continuum mechanical calculation of the lithiation-induced stress field distribution for the silicon particles embedded in carbon fibers (using a silicon core and carbon shell model). (a) Core–shell spherical model of silicon wrapped by carbon film; (b) dependence of the radial stress on the thickness of the charged layer; (c) dependence of the hoop stresses on the thickness of the charged layer. In the calculation, the following parameters were used: the elastic constants of silicon are C_{11}= 166 GPa, C_{12} = 64 GPa, C_{44} = 79.6 GPa; the elastic constants of carbon are C_{11} = 859 GPa, C_{12} = 118 GPa, C_{44} = 36 GPa, R_0 = 60 nm, R = 120 nm, and 300% volume expansion upon lithiation of silicon to Li_xSi.

the battery. In addition, the newly formed fracture surface would consume the electrolyte when forming a solid–electrolyte interface layer in the freshly fracture surfaces. Furthermore, the generation of the new SEI layer would trap more lithium and reduce the rechargeable capacity. Therefore, the fracture of the carbon nanofiber has a detrimental effect on the battery performance. The observed lithiation behavior and structural evolution of the silicon nanoparticle attached to and embedded in a CNF may guide a better design of the composite anode based on silicon and carbon. Although embedding silicon nanoparticles may lead to a good electrical contact between the particle and the carbon fiber, the inherent delayed lithiation and fracture of the carbon fiber will be undoubtedly detrimental to the charging rate and capacity retention and ultimately lead to the failure of the battery. It may be argued that a strong carbon material, such as graphene, may prevent the fracture of the carbon. However, a strong confinement of the carbon layer on the lithiation of silicon is not clear. One ideal configuration could be confining silicon nanoparticles in a hollow carbon shell or embedding silicon nanoparticles in deformable carbon materials. This type of structure allows the free expansion of the silicon particle upon lithiation, while maintaining the interface between the anode and the electrolyte upon cyclic charge/discharge of the battery. Representative examples along this line of optimized microstructural design concepts include yolk–shell,[59] core–shell,[60–62] and embedding of silicon nanoparticles in a conductive polymer.[63] The observation of contact flattening of aggregated particles appears to be equivalent to the coarsening of the particles, which leads to the increase of the transport distance of the lithium ions during the charge and discharge process. Therefore, it is essential to avoid the aggregation of silicon nanoparticles in the composite materials.

CONCLUSION

Silicon and carbon are two important components for designing high-capacity anode materials for lithium ion batteries. The lithiation behavior and the response of such a composite system to the volume change of silicon nanoparticles depend on the spatial correlation of the silicon nanoparticle and the carbon materials. Embedding silicon nanoparticles in a carbon matrix will lead to the delayed lithiation of the silicon as compared with the particles attached to the carbon fiber, therefore limiting the rate performance of the battery. Lithiation of aggregated silicon nanoparticles shows contact flattening, which is characteristically analogous to the classic sintering of powder particles by a neck-growth mechanism, therefore increasing lithium diffusion distances. Lithiation of silicon nanoparticles embedded in a carbon matrix will lead to a high stress field, which can lead to the fracture of the carbon fiber. Therefore, in designing the silicon

nanoparticles and carbon-based nanocomposites for high capacity anode applications, a proper spatial correlation of the silicon nanoparticle with the carbon matrix is very important.

METHODS

Si nanoparticles and a carbon nanofiber (Si-CNF) composite were prepared by the electrospin method. A detailed description of the sample preparation is reported in previous publications.[35,64] For this work, the loading of the Si nanoparticles in the carbon nanofiber is 10 wt % (silicon relative to the carbon precursor). Microstructural evolution of the Si-CNF composite during the charge/discharge is studied *in situ* using a nanobattery configuration with a single Si-CNF as anode, $LiCoO_2$ as the cathode, and ionic liquid based electrolyte (ILE, 10 wt % lithium bis(trifluoromethylsulfonyl)imide dissolved in 1-butyl-1-methylpyrrolidinium bis(trifluoromethylsulfonyl)-imide) as reported previously.[15−17] In making the nanobattery, a few Si-CNF were attached to a gold rod with conductive silver epoxy. A piece of $LiCoO_2$ powder compact was attached to a gold rod serving as the cathode. One drop of the ILE was placed on the surface of the $LiCoO_2$ film as the electrolyte. A constant potential of −4.0 V was applied to the Si-CNF fiber against $LiCoO_2$ upon charging (lithiation) and 0 V upon discharging (delithiation). All the *in situ* electrochemical tests were conducted on a Titan 80−300 kV scanning/transmission electron microscope operated at 300 kV with a Nanofactory TEM scanning tunneling microscopy holder.

Conflict of Interest: The authors declare no competing financial interest.

Acknowledgment. This work was supported by the Laboratory Directed Research and Development (LDRD) program at the Pacific Northwest National Laboratory (PNNL). This work was conducted in the William R. Wiley Environmental Molecular Sciences Laboratory (EMSL), a national scientific user facility sponsored by DOE's Office of Biological and Environmental Research and located at PNNL. PNNL is operated by Battelle for the Department of Energy under Contract DE-AC05-76RLO1830.

Supporting Information Available: Supporting movies showing the lithation behavior of Si particles attached to and embedded in a carbon fiber and the fracture of the carbon fiber induced by the lithiation of the embedded Si nanoparticles, additional SEM and TEM images showing single Si particles attached to the CNF surface, and the method for the calculation of the stress field based on the silicon core and carbon shell model. These materials are available free of charge *via* the Internet at http://pubs.acs.org.

REFERENCES AND NOTES

1. Zhao, K.; Wang, W. L.; Gregoire, J.; Pharr, M.; Suo, Z.; Vlassak, J. J.; Kaxiras, E. Lithium-Assisted Plastic Deformation of Silicon Electrodes in Lithium-Ion Batteries: A First-Principles Theoretical Study. *Nano Lett.* **2011**, *11*, 2962–2967.
2. Zhang, T.; Zhang, H. P.; Yang, L. C.; Wang, B.; Wu, Y. P.; Takamura, T. The Structural Evolution and Lithiation Behavior of Vacuum-Deposited Si Film with High Reversible Capacity. *Electrochim. Acta* **2008**, *53*, 5660–5664.
3. Song, T.; Xia, J.; Lee, J.-H.; Lee, D. H.; Kwon, M.-S.; Choi, J.-M.; Wu, J.; Doo, S. K.; Chang, H.; Park, W. I.; *et al*. Arrays of Sealed Silicon Nanotubes as Anodes for Lithium Ion Batteries. *Nano Lett.* **2010**, *10*, 1710–1716.
4. Qu, J.; Li, H.; Henry, J. J., Jr; Martha, S. K.; Dudney, N. J.; Xu, H.; Chi, M.; Lance, M. J.; Mahurin, S. M.; Besmann, T. M.; *et al*. Self-Aligned Cu−Si Core−Shell Nanowire Array as a High-Performance Anode for Li-Ion Batteries. *J. Power Sources* **2012**, *198*, 312–317.
5. Liu, X. H.; Zhang, L. Q.; Zhong, L.; Liu, Y.; Zheng, H.; Wang, J. W.; Cho, J.-H.; Dayeh, S. A.; Picraux, S. T.; Sullivan, J. P.; *et al*. Ultrafast Electrochemical Lithiation of Individual Si Nanowire Anodes. *Nano Lett.* **2011**, *11*, 2251–2258.
6. Liu, N.; Hu, L.; McDowell, M. T.; Jackson, A.; Cui, Y. Prelithiated Silicon Nanowires as an Anode for Lithium Ion Batteries. *ACS Nano* **2011**, *5*, 6487–6493.
7. Johari, P.; Qi, Y.; Shenoy, V. B. The Mixing Mechanism During Lithiation of Si Negative Electrode in Li-Ion Batteries: An *ab Initio* Molecular Dynamics Study. *Nano Lett.* **2011**, *11*, 5494–5500.
8. Ghassemi, H.; Au, M.; Chen, N.; Heiden, P. A.; Yassar, R. S. *In Situ* Electrochemical Lithiation/Delithiation Observation of Individual Amorphous Si Nanorods. *ACS Nano* **2011**, *5*, 7805–7811.
9. Cui, L.-F.; Ruffo, R.; Chan, C. K.; Peng, H.; Cui, Y. Crystalline-Amorphous Core−Shell Silicon Nanowires for High Capacity and High Current Battery Electrodes. *Nano Lett.* **2008**, *9*, 491–495.
10. Liu, X. H.; Zheng, H.; Zhong, L.; Huang, S.; Karki, K.; Zhang, L. Q.; Liu, Y.; Kushima, A.; Liang, W. T.; Wang, J. W.; *et al*. Anisotropic Swelling and Fracture of Silicon Nanowires During Lithiation. *Nano Lett.* **2011**, *11*, 3312–3318.
11. Lee, S. W.; McDowell, M. T.; Choi, J. W.; Cui, Y. Anomalous Shape Changes of Silicon Nanopillars by Electrochemical Lithiation. *Nano Lett.* **2011**, *11*, 3034–3039.
12. Chan, C. K.; Peng, H.; Liu, G.; McIlwrath, K.; Zhang, X. F.; Huggins, R. A.; Cui, Y. High-Performance Lithium Battery Anodes Using Silicon Nanowires. *Nat. Nanotechnol.* **2008**, *3*, 31–35.
13. Lee, S. W.; McDowell, M. T.; Berla, L. A.; Nix, W. D.; Cui, Y. Fracture of Crystalline Silicon Nanopillars During Electrochemical Lithium Insertion. *Proc. Natl. Acad. Sci. U. S. A.* **2012**, *109*, 4080–4085.
14. Yang, H.; Huang, S.; Huang, X.; Fan, F. F.; Liang, W.; Liu, X. H.; Chen, L. Q.; Huang, J. Y.; Li, J.; Zhu, T.; *et al*. Orientation-Dependent Interfacial Mobility Governs the Anisotropic Swelling in Lithiated Silicon Nanowires. *Nano Lett.* **2012**, *12*, 1953–1958.
15. Jeong, G.; Lee, S. M.; Choi, N. S.; Kim, Y.-U.; Lee, C. K. Stabilizing Dimensional Changes in Si-Based Composite Electrodes by Controlling the Electrode Porosity: An *in Situ* Electrochemical Dilatometric Study. *Electrochim. Acta* **2011**, *56*, 5095–5101.
16. Cui, L.-F.; Hu, L.; Wu, H.; Choi, J. W.; Cui, Y. Inorganic Glue Enabling High Performance of Silicon Particles as Lithium Ion Battery Anode. *J. Electrochem. Soc.* **2011**, *158*, A592–A596.
17. Chakrapani, V.; Rusli, F.; Filler, M. A.; Kohl, P. A. Silicon Nanowire Anode: Improved Battery Life with Capacity-Limited Cycling. *J. Power Sources* **2012**, *205*, 433–438.
18. Baranchugov, V.; Markevich, E.; Pollak, E.; Salitra, G.; Aurbach, D. Amorphous Silicon Thin Films as a High Capacity Anodes for Li-Ion Batteries in Ionic Liquid Electrolytes. *Electrochem. Commun.* **2007**, *9*, 796–800.
19. Yao, Y.; McDowell, M. T.; Ryu, I.; Wu, H.; Liu, N.; Hu, L.; Nix, W. D.; Cui, Y. Interconnected Silicon Hollow Nanospheres for Lithium-Ion Battery Anodes with Long Cycle Life. *Nano Lett.* **2011**, *11*, 2949–2954.
20. Wu, H.; Chan, G.; Choi, J. W.; Ryu, I.; Yao, Y.; McDowell, M. T.; Lee, S. W.; Jackson, A.; Yang, Y.; Hu, L. B.; *et al*. Stable Cycling of Double-Walled Silicon Nanotube Battery Anodes through Solid−Electrolyte Interphase Control. *Nat. Nanotechnol.* **2012**, *7*, 310–315.
21. Tibbetts, G. G. Why Are Carbon Filaments Tubular. *J. Cryst. Growth* **1984**, *66*, 632–638.
22. Tibbetts, G. G.; Lake, M. L.; Strong, K. L.; Rice, B. P. A Review of the Fabrication and Properties of Vapor-Grown Carbon Nanofiber/Polymer Composites. *Compos. Sci. Technol.* **2007**, *67*, 10.
23. Geim, A. K. Graphene: Status and Prospects. *Science* **2009**, *324*, 1530–1534.
24. Cui, L. F.; Yang, Y.; Hsu, C. M.; Cui, Y. Carbon-Silicon Core-Shell Nanowires as High Capacity Electrode for Lithium Ion Batteries. *Nano Lett.* **2009**, *9*, 3370–3374.

25. Cui, L. F. H.; Hu, L. B.; J., L.; Choi, J. W.; Cui, Y. Light-Weight Free-Standing Carbon Nanotube-Silicon Films for Anodes of Lithium Ion Batteries. *ACS Nano* **2010**, *4*, 3671–3678.
26. Wang, W.; Kumta, P. N. Nanostructured Hybrid Silicon/Carbon Nanotube Heterostructures: Reversible High-Capacity Lithium-Ion Anodes. *ACS Nano* **2010**, *4*, 2233–2241.
27. Hu, L.; Wu, H.; Gao, Y.; Cao, A.; Li, H.; McDough, J.; Xie, X.; Zhou, M.; Cui, Y. Silicon-Carbon Nanotube Coaxial Sponge as Li-Ion Anodes with High Areal Capacity. *Adv. Energy Mater.* **2011**, *1*, 523–527.
28. Ng, S. H.; Wang, J.; Wexler, D.; Chew, S. Y.; Liu, H. K. Amorphous Carbon-Coated Silicon Nanocomposites: A Low-Temperature Synthesis *via* Spray Pyrolysis and Their Application as High-Capacity Anodes for Lithium-Ion Batteries. *J. Phys. Chem. C* **2007**, *111*, 11131–11138.
29. Yang, J.; Wang, B. F.; Wang, K.; Liu, Y.; Xie, J. Y.; Wen, Z. S. Si/C Composites for High Capacity Lithium Storage Materials. *Electrochem. Solid State* **2003**, *6*, A154–A156.
30. Xue, J. S.; Myrtle, K.; Dahn, J. R. An Epoxy-Silane Approach to Prepare Anode Materials for Rechargeable Lithium Ion Batteries. *J. Electrochem. Soc.* **1995**, *142*, 2927–2935.
31. Jang, S. M.; Miyawaki, J.; Tsuji, M.; Mochida, I.; Yoon, S. H. The Preparation of a Novel Si-CNF Composite as an Effective Anodic Material for Lithium-Ion Batteries. *Carbon* **2009**, *47*, 3383–3391.
32. Cui, L. F.; Ruffo, R.; Chan, C. K.; Peng, H. L.; Cui, Y. Crystalline-Amorphous Core-Shell Silicon Nanowires for High Capacity and High Current Battery Electrodes. *Nano Lett.* **2009**, *9*, 491–495.
33. Xiang, H.; Zhang, K.; Ji, G.; Lee, J. Y.; Zou, C.; Chen, X.; Wu, J. Graphene/Nanosized Silicon Composites for Lithium Battery Anodes with Improved Cycling Stability. *Carbon* **2011**, *49*, 1787–1796.
34. Wang, C.-M.; Li, X.; Wang, Z.; Xu, W.; Liu, J.; Gao, F.; Kovarik, L.; Zhang, J.-G.; Howe, J.; Burton, D. J.; *et al*. *In Situ* TEM Investigation of Congruent Phase Transition and Structural Evolution of Nanostructured Silicon/Carbon Anode for Lithium Ion Batteries. *Nano Lett.* **2012**, *12*, 1624–1632.
35. Ji, L.; Zhang, X. Electrospun Carbon Nanofibers Containing Silicon Particles as an Energy-Storage Medium. *Carbon* **2009**, *47*, 3219–3226.
36. Hwang, T. H.; Lee, Y. M.; Kong, B. S.; Seo, J. S.; Choi, J. W. Electrospun Core−Shell Fibers for Robust Silicon Nanoparticle-Based Lithium Ion Battery Anodes. *Nano Lett.* **2012**, *12*, 802–807.
37. Huang, J. Y.; Zhong, L.; Wang, C. M.; Sullivan, J. P.; Xu, W.; Zhang, L. Q.; Mao, S. X.; Hudak, N. S.; Liu, X. H.; Subramanian, A.; *et al*. *In Situ* Observation of the Electrochemical Lithiation of a Single SNO_2 Nanowire Electrode. *Science* **2010**, *330*, 1515–1520.
38. Wang, C. M.; Xu, W.; Liu, J.; Choi, D. W.; Arey, B.; Saraf, L. V.; Zhang, J. G.; Yang, Z. G.; Thevuthasan, S.; Baer, D. R.; *et al*. *In Situ* Transmission Electron Microscopy and Spectroscopy Studies of Interfaces in Li Ion Batteries: Challenges and Opportunities. *J. Mater. Res.* **2010**, *25*, 1541–1547.
39. Limthongkul, P.; Jang, Y. I.; Dydney, N. J.; Chiang, Y. M. Electrochemically-Driven Solid-State Amorphization in Lithium-Silicon Alloys and Implications for Lithium Storage. *Acta Mater.* **2003**, *51*, 1103–1113.
40. Zhao, K. J.; Pharr, M.; Wan, Q.; Wang, W. L.; Kaxiras, E.; Vlassak, J. J.; Suo, Z. G. Concurrent Reaction and Plasticity During Initial Lithiation of Crystalline Silicon in Lithium-Ion Batteries. *J. Electrochem. Soc.* **2012**, *159*, A238–A243.
41. Chon, M. J.; Sethuraman, V. A.; McCormick, A.; Srinivasan, V.; Guduru, P. R. Real-Time Measurement of Stress and Damage Evolution During Initial Lithiation of Crystalline Silicon. *Phys. Rev. Lett.* **2011**, *107*, 045503.
42. Deshpande, R.; Cheng, Y.-T.; Verbrugge, M. W.; Timmons, A. Diffusion Induced Stresses and Strain Energy in a Phase-Transforming Spherical Electrode Particle. *J. Electrochem. Soc.* **2011**, *158*, A718–A724.
43. Wakai, F.; Yoshida, M.; Shinoda, Y.; Akatsu, T. Coarsening and Grain Growth in Sintering of Two Particles of Different Sizes. *Acta Mater.* **2005**, *53*, 1361–1371.
44. Pokluda, O.; Bellehumeur, C. T.; Vlachopoulos, J. Modification of Frenkel's Model for Sintering. *AIChE J.* **1997**, *43*, 3253–3256.
45. Wakai, F.; Aldinger, F. Sintering Forces in Equilibrium and Non-Equilibrium States. *Sci. Tech. Adv. Mater.* **2004**, *5*, 521–525.
46. Frenkel, J. Viscous Flow of Crystalliine Bodies under the Action of Surface Tension. *J. Phys. USSR* **1945**, *9*, 385–391.
47. Kingery, W. D.; Berg, M. Study of the Initial Stages of Sintering Solids by Viscous Flow, Evaporation-Condensation, and Self-Diffusion. *J. Appl. Phys.* **1955**, *26*, 1205–1212.
48. Karki, K.; Epstein, E.; Cho, J. H.; Jia, Z.; Li, T.; Picraux, T.; Wang, C. S.; Cumings, J. Lithium-Assisted Electrochemical Welding in Silicon Nanowire Battery Electrodes. *Nano Lett.* **2012**, *12*, 1392–1397.
49. Liu, X. H.; Huang, S.; Picraux, S. T.; Li, J.; Zhu, T.; Huang, J. Y. Reversible Nanopore Formation in Ge Nanowires During Lithiation Delithiation Cycling: An *in Situ* Transmission Electron Microscopy Study. *Nano Lett.* **2011**, *11*, 3991–3997.
50. Choi, J. W.; McDough, J.; Jeong, S.; Yoon, J. S.; Chan, C. K.; Cui, Y. Stepwise Nanopore Evolution in One-Dimensional Nanostructures. *Nano Lett.* **2010**, *10*, 1409–1413.
51. McDowell, M. T.; Lee, S. W.; Ryu, I.; Wu, H.; Nix, W. D.; Choi, J. W.; Cui, Y. Novel Size and Surface Oxide Effects in Silicon Nanowires as Lithium Battery Anodes. *Nano Lett.* **2011**, *11*, 4018–4025.
52. Ryu, I.; Choi, J. W.; Cui, Y.; Nix, W. D. Size-Dependent Fracture of Si Nanowire Battery Anodes. *J. Mech. Phys. Solids* **2011**, *59*, 1717–1730.
53. Liu, Y.; Zheng, H.; Liu, X. H.; Huang, S.; Zhu, T.; Wang, J. W.; Kushima, A.; Hudak, N. S.; Huang, X.; Zhang, S. L.; *et al*. Lithiation-Induced Embrittlement of Multiwalled Carbon Nanotubes. *ACS Nano* **2011**, *5*, 7245–7253.
54. Liu, X. H.; Zhang, L. Q.; Zhong, L.; Liu, Y.; Zheng, H.; Wang, J. W.; Cho, J. H.; Dayeh, S. A.; Picraux, S. T.; Sullivan, J. P.; *et al*. Ultrafast Electrochemical Lithiation of Individual Si Nanowire Anodes. *Nano Lett.* **2011**, *11*, 2251–2258.
55. Yang, H.; Bang, H. J.; Prakash, J. Evaluation of Electrochemical Interface Area and Lithium Diffusion Coefficient for a Composite Graphite Anode. *J. Electrochem. Soc.* **2004**, *151*, A1247–A1250.
56. Shim, J.; Striebel, K. A. Electrochemical Characterization of Thermally Oxidized Natural Graphite Anodes in Lithium Ion Batteries. *J. Power Sources* **2007**, *164*, 862–867.
57. Persson, K.; Sethuraman, V. A.; Hardwick, L. J.; Hinuma, Y.; Meng, Y. S.; va der Ven, A.; Srinivasan, V.; Kostecki, R.; Ceder, G. Lithium Diffusion in Graphitic Carbon. *J. Phys. Chem. Lett.* **2010**, 1176–1180.
58. Liu, X. H.; Zhong, L.; Huang, S.; Mao, S. X.; Zhu, T.; Huang, J. Y. Size-Dependent Fracture of Silicon Nanoparticles During Lithiation. *ACS Nano* **2012**, *6*, 1522–1531.
59. Liu, N.; Wu, H.; McDowell, M. T.; Yao, Y.; Wang, C. M.; Cui, Y. A York-Shell Design for Stabilized and Scalable Li-Ion Battery Alloy Anodes. *Nano Lett.* **2012**, *12*, 3315–3321.
60. Jeong, H. M.; Lee, S. Y.; Shin, W. H.; Kwon, J. H.; Shakoor, A.; Hwang, T. H.; Kim, S. Y.; Kong, B.-S.; Seo, J.-S.; Lee, Y. M.; *et al*. Silicon@Porous Nitrogen-Doped Carbon Spheres through a Bottom-up Approach Are Highly Robust Lithium-Ion Battery Anodes. *RSC Adv.* **2012**, *2*, 4311–4317.
61. Zhou, X.; Yin, Y.-X.; Cao, A.-M.; Wan, L.-J.; Guo, Y.-G. Efficient 3D Conducting Networks Built by Graphene Sheets and Carbon Nanoparticles for High-Performance Silicon Anode. *ACS Appl. Mater. Interfaces* **2012**, *4*, 2824–2828.
62. Lee, B.-S.; Son, S.-B.; Park, K.-M.; Seo, J.-H.; Lee, S.-H.; Choi, I.-S.; Oh, K.-H.; Yu, W.-R. Fabrication of Si Core/C Shell Nanofibers and Their Electrochemical Performances as a Lithium-Ion Battery Anode. *J. Power Sources* **2012**, *206*, 267–273.
63. Liu, G.; Xun, S.; Vukmirovic, N.; Song, X. Y.; Olalde-Velasco, P.; Zheng, H. H.; Battaglia, V. S.; Wang, L. W.; Yang, W. L. Polymers with Tailored Electronic Structure for High

Capacity Lithium Battery Electrodes. *Adv. Mater.* **2011**, *23*, 4679–4683.
64. Ji, L.; Zhang, X. Evaluation of Si/Carbon Composite Nanofiber-Based Insertion Anodes for New-Generation Rechargeable Lithium-Ion Batteries. *Energy Environ. Sci.* **2010**, *3*, 124–129.